RAA 2019 Vol. **19** No. **5**, 67(10pp) doi: 10.1088/1674–4527/19/5/67

http://www.raa-journal.org *http://iopscience.iop.org/raa*

***R**esearch in*
***A**stronomy and*
***A**strophysics*

Transition-region explosive events produced by plasmoid instability

Dong Li

Key Laboratory of Dark Matter and Space Astronomy, Purple Mountain Observatory, Chinese Academy of Sciences, Nanjing 210034, China; *lidong@pmo.ac.cn*
Key Laboratory of Solar Activity, National Astronomical Observatories, Chinese Academy of Sciences, Beijing 100101, China

Received 2018 July 1; accepted 2018 November 5

Abstract Magnetic reconnection is thought to be a key process in most solar eruptions. Thanks to high-resolution observations and simulations, the studied scale of the reconnection process has become smaller and smaller. Spectroscopic observations show that the reconnection site can be very small, which always exhibits a bright core and two extended wings with fast speeds, i.e., transition-region explosive events. In this paper, using the PLUTO code, we perform a 2-D magnetohydrodynamic simulation to investigate small-scale reconnection in double current sheets. Based on our simulation results, such as the line-of-sight velocity, number density and plasma temperature, we can synthesize the line profile of Si IV 1402.77 Å which is a well known emission line used to study transition-region explosive events on the Sun. The synthetic line profile of Si IV 1402.77 Å is complex with a bright core and two broad wings which can extend to nearly 200 km s^{-1}. Our simulation results suggest that the transition-region explosive events on the Sun are produced by plasmoid instability during small-scale magnetic reconnection.

Key words: Sun: transition region — line: profiles — methods: numerical — magnetohydrodynamics (MHD)

1 INTRODUCTION

The breaking and re-joining of magnetic fields are generally thought to be the process of magnetic reconnection. It is believed to be a basic process of energy release on the Sun, and is usually accompanied by particle acceleration. Almost all solar eruptions which are related to magnetic energy release are thought to be associated with magnetic reconnection, i.e., coronal mass ejections (Lin et al. 2005; Guo et al. 2013), emerging flux regions (Zhao & Li 2012; Yang & Zhang 2014), bipolar magnetic regions (Jiang et al. 2014; Li 2017), solar flares (Petschek 1964; Liu et al. 2010; Yan et al. 2018), solar filaments (Shen et al. 2015; Li et al. 2016b; Li & Ding 2017), bright points (Priest et al. 1994; Li & Ning 2012; Zhao et al. 2017) and transition-region explosive events (Innes et al. 1997; Ning et al. 2004; Huang et al. 2017). That is to say, the Sun can provide various observational features of magnetic reconnection in a wide range of scales, i.e., from ∼1000 Mm to ∼1 Mm. The diagnostics of magnetic reconnection often depend on the associated imaging observations (Masuda et al. 1994; Tian et al. 2014; Xue et al. 2016), spectroscopic observations (Curdt & Tian 2011; Cheng et al. 2015; Li et al. 2018; Tian et al. 2018) and also magnetohydrodynamic (MHD) simulations (Jin et al. 1996; Khomenko & Collados 2012; Yang et al. 2015a). Over the past few decades, many observational features have been identified as evidence for magnetic reconnection on the Sun, such as X-type structures (Aschwanden 2002; Su et al. 2013; Yang et al. 2015b), magnetic null points (Sun et al. 2012; Zhang et al. 2012), current sheets (Lin et al. 2005; Liu et al. 2010; Xue et al. 2018), reconnection inflows or outflows (Liu et al. 2013; Ning & Guo 2014; Sun et al. 2015; Li et al. 2016a), highly energetic particles (Li et al. 2007, 2009; Klassen et al. 2011) and also bi-directional jets (Dere et al. 1991; Winebarger et al. 2002; Innes & Teriaca 2013; Hong et al. 2016).

Transition-region explosive events are detected frequently in the quiet or active Sun. They usually manifest as broad non-Gaussian profiles with a high velocity of about

100 km s^{-1} in the emission lines, i.e., Si IV 1393 Å (Innes et al. 1997; Ning et al. 2004), 1402.77 Å (Huang et al. 2014; Innes et al. 2015), C IV 1548 Å and O IV 1032 Å (Pérez et al. 1999; Innes & Teriaca 2013). Usually, these emission lines are formed between 6×10^4 K (e.g., C III) and 7×10^5 K (e.g., Ne VIII) (Wilhelm et al. 2007) in the transition regions. Transition-region explosive events were first detected in spectra observed by the High Resolution Telescope and Spectrograph (HRTS) (Brueckner & Bartoe 1983), and then described in more detail by Dere et al. (1989) and Dere (1994). Their typical size is found to be about 1500 km and their lifetime is around 60 s. Spectroscopic observations (e.g., Dere et al. 1989; Innes et al. 1997; Ning et al. 2004) further show that they always exhibit a line asymmetry, i.e., extended blue or red wings, whose typical speed can be $\sim$100 km s^{-1}. A single event observed by a line profile often exhibits blue and red shifts simultaneously, which is regarded as a small-scale bi-directional jet in the transition region, and it is thought to be associated with small-scale magnetic reconnection on the Sun (Innes et al. 1997).

MHD numerical simulations have been applied to magnetic reconnection in the corona (Shen et al. 2011; Ni et al. 2012), transition region (e.g., Innes & Tóth 1999; Sarro et al. 1999; Roussev et al. 2001) and chromosphere or even photosphere (Ni et al. 2015, 2016) on the Sun. Previous simulations of the transition-region explosive events were often based on the Petschek mechanism (Petschek 1964). The upward and downward motions of magnetic islands were thought to be associated with blue and red shifts in the explosive events (Jin et al. 1996). Further simulation (Roussev et al. 2001) indicated that the reconnection with an X-point in the transition region produced a large blue shift ($\sim$100 km s^{-1}) but a small red shift. Meanwhile, Innes & Tóth (1999) performed compressible MHD simulations of small-scale explosive events based on the Petschek model, and they found that these simulations could reproduce well the blue or red shifts with high velocities, but failed to explain the bright core near the line center with low velocities observed in the spectra (e.g., Dere et al. 1991; Innes 2001). Based on large-scale MHD simulations (e.g., Bhattacharjee et al. 2009; Heggland et al. 2009; Huang & Bhattacharjee 2010; Huang et al. 2017), magnetic reconnection that proceeds via plasmoid instability has been proposed. Now, this model has also been applied to explain the small-scale explosive events which exhibit brightening both at the spectral line core and two extended wings, i.e., the line profile of Si IV 1402.77 Å (e.g., Innes et al. 2015).

In this paper, we perform a small-scale 2-D MHD simulation of magnetic reconnection which is produced in double current sheets with the PLUTO code (Mignone et al. 2007, 2012). We also synthesize the line profiles which form in the transition region, i.e., Si IV 1402.77 Å (Tian 2017). Our result suggests that the transition-region explosive events on the Sun are the small-scale reconnection sites, which are consistent with *Interface Region Imaging Spectrograph* (*IRIS*) (De Pontieu et al. 2014) observations (see Innes et al. 2015).

2 NUMERICAL METHOD

2.1 MHD Simulation

In this paper, the PLUTO code (Mignone et al. 2007) with adaptive mesh refinement (AMR) (Mignone et al. 2012) is applied to perform the MHD simulation. Briefly, a Newtonian fluid with density (ρ), velocity ($\boldsymbol{v}$) and magnetic field ($\boldsymbol{B}$) is considered, then the forms of single-fluid MHD equations are

$$\begin{aligned}
&\frac{\partial \rho}{\partial t} + \nabla\cdot(\rho\boldsymbol{v}) = 0,\\
&\frac{\partial(\rho\boldsymbol{v})}{\partial t} + \nabla\cdot(\rho\boldsymbol{v}\boldsymbol{v} - \boldsymbol{B}\boldsymbol{B}) + \nabla p_t = 0,\\
&\frac{\partial E}{\partial t} + \nabla\cdot[(E+p_t)\boldsymbol{v} - (\boldsymbol{v}\cdot\boldsymbol{B})\boldsymbol{B}] = -\eta\cdot\boldsymbol{J}\times\boldsymbol{B} - \Lambda,\\
&\frac{\partial \boldsymbol{B}}{\partial t} - \nabla\times(\boldsymbol{v}\times\boldsymbol{B}) = -\nabla\times(\eta\boldsymbol{J}),
\end{aligned} \tag{1}$$

where $p_t = p + \boldsymbol{B}^2/2$ is the total pressure which consists of thermal and magnetic pressures. $E = p/(\gamma-1) + \frac{1}{2}\rho\boldsymbol{v}^2 + \frac{1}{2}\boldsymbol{B}^2$ is the total energy density at the ideal state, and γ is the specific heat ratio. $\boldsymbol{J} = \nabla\times\boldsymbol{B}$ is the electric current density and η is the resistivity. Our simulation considers Ohmic heating and optically thin radiative cooling (see Eq. (2)), but dissipative effects caused by viscosity and gravity are ignored. Notice that only hydrogen gas is considered in our 2-D MHD model.

$$\Lambda = n^2\tilde{\Lambda}(T), \quad \text{with} \quad n = \frac{\rho}{\mu m_u}. \tag{2}$$

Here n is the number density, μ is the mean molecular weight and m_u is the atomic mass unit. In our model, the cooling rates ($\tilde{\Lambda}$) are discrete. Figure 1 displays the cooling rates (see Mignone et al. 2007) used in this paper.

In our simulation, we consider a Cartesian 2-D uniform grid x, $y \in$ [0, 2], with 64 $\times$ 64 zones at the coarse level, and with periodic boundary conditions along both of the two directions. To trigger the magnetic reconnection,

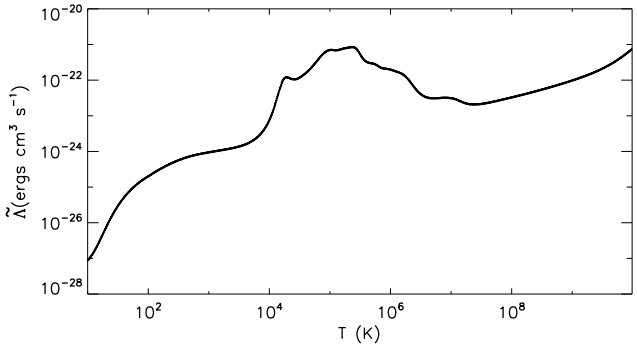

Fig. 1 Tabulated cooling rates in log−log space. The data are derived from Mignone et al. (2007).

the initial magnetic field is defined only in the vertical (y) direction, as shown in Equation (3) with $B = 1.0$ (see Mignone et al. 2012).

$$B_y = \begin{cases} -B & \text{if} \quad |x-1| \leq 0.5 \\ B & \text{otherwise} \end{cases} . \qquad (3)$$

In the x direction, a small initial perturbation to the velocity is set to start the reconnection, i.e., $v_x = 0.1 \times v_0 \sin(\pi \cdot y)$. The initial thermal pressure is given by the magnetic field and plasma beta (β), such as $p = \beta \cdot B^2/2$. The MHD fluid has a uniform density at the beginning, which is $\rho = 1.0$. The temperature can be obtained from the density and thermal pressure in the code, i.e., $T = p/\rho$. In order to obtain the high-resolution grid and save computing time, AMR is allowed for the MHD simulation. Four-level refinement is initiated for carrying out the integration with the TVDLF solver. Finally, we perform reconstruction on characteristic variables rather than primitive values and set the monotonized central difference limiter (MC_LIM). In the whole simulation, we assume an ideal gas state with a specific heat ratio (γ) of 5/3 and mean molecular weight (μ) of 1/2.

Generally speaking, PLUTO works with non-dimensional (or coded) units, which are described above. However, we have considered the radiative cooling process, and dimensional constants are essential to scale data values to physical units. Thus, we have to introduce the specific length and energy scale so that they can be compared with dynamical advection scales. Therefore, we can specify three fundamental units. They are the length (L_0), velocity (v_0) and number density (n_0) which correspond to a mass density of $\rho_0 = n_0 m_u$. The other units can be derived from these three fundamental units, such as time $t_0 = L_0/v_0$, pressure $p_0 = \rho_0 v_0^2$, magnetic field $B_0 = v_0\sqrt{4\pi\rho_0}$ and temperature $T_0 = \mu m_u v_0^2/k_{\rm B}$, where $k_{\rm B}$ is the Boltzmann constant. We note that all these dimensional units are in the c.g.s. system, i.e., cm, s and g. During the entire process of MHD simulation, a uniform resistivity (η) is employed.

Table 1 lists the characteristic and initial values of these fundamental units in our 2-D simulation. The characteristic length is set to be 10^8 cm, and thus the simulation box has a size of 2×2 Mm. The characteristic number density and velocity are set to be 10^{10} cm^{-3} and 2×10^7 cm s^{-1} at first, respectively, which lead to a characteristic plasma beta of $\beta \approx 1.67$, as shown in the second line (CPs) of Table 1. Therefore, the MHD flows have an initial uniform density of 10^{10} cm^{-3}, an initial magnetic field of about 10 G and a small initial perturbation velocity of 2×10^6 cm s^{-1}. This gives an initial plasma beta of $\beta \approx 0.02$, as indicated in the third line (IPs) of Table 1. Finally, a uniform resistivity ($\eta = 10^{-5}$) is applied.

2.2 Line Synthesis

The values of six variables, including number density (n), total energy (E), velocities (v_x, v_y) and magnetic fields (B_x, B_y) are derived at each time step by solving the 2-D MHD equations, then the plasma temperature (T) can be derived by inserting the values of these variables. Using these variables and assuming that the emission line is composed of a group of Gaussian profiles, we can synthesize the line profile with Equation (4) (see also Hansteen et al. 2010; Yuan et al. 2016), i.e., Si IV 1402.77 Å, which is a well known spectral line to study the transition-region explosive events from *IRIS* observations (e.g., Innes et al. 2015).

$$I(v) = \frac{\Sigma}{4\pi R_{AU}^2} \int \phi(v_s)\, n_e\, n\, g(T) ds. \qquad (4)$$

Here the integrated intensity of the spectral line is carried out along the chosen light-of-sight (LOS). n_e is the electron number density, and assuming that $n_e = n$, Σ is the area of the MHD simulation region, R_{AU} is the distance between the Sun and the Earth, and $\frac{\Sigma}{4\pi R_{AU}^2}$ repre-

Table 1 The Characteristic Parameters (CPs) and Initial Parameters (IPs) in Our 2-D MHD Simulations

	L_0 (cm)	n_0 (cm^{-3})	v_0 (cm s^{-1})	T_0 (K)	B_0 (G)	β	η
CPs	10^8	10^{10}	2×10^7	2.4×10^6	$\sim$10	1.67	10^{-5}
IPs	10^8	10^{10}	2×10^6	2.4×10^4	$\sim$10	0.02	10^{-5}

sents the ratio between the spectral line intensity which radiates from the Sun and that we receive on the Earth (e.g., Winebarger et al. 1999). $g(T)$ is the contribution function of the specified emission line, i.e., Si IV 1402.77 Å, which can be obtained from the CHIANTI database version 8.0 (Del Zanna et al. 2015). $\phi(v_s)$ is a Gaussian function with variable v_s (the unit of velocity here is km s^{-1}), see Equation (5).

$$\phi(v_s) = \frac{1}{\sqrt{\pi}\Delta v_D} e^{-\frac{(v-v_s)^2}{2\Delta v_D^2}}, \quad \text{with} \quad \Delta v_D = \sqrt{\frac{2k_{\rm B}T}{m}}. \tag{5}$$

Here Δv_D represents the thermal broadening from the simulation temperature T, and m is the mass of the radiating ion, while v_s is the fluid speed projected along the LOS direction, i.e., velocity in the y direction (v_y) from the numerical results, as shown in Figure 2.

3 RESULTS

3.1 MHD Simulation Results

Figure 2 shows the variables which are derived from our 2-D MHD simulation at $t = 22$ s. The upper panels display the simulation variables without the radiative cooling process, such as the velocities along the y direction (v_y), plasma temperature (T) and number density (n_e). All these simulation variables demonstrate that every magnetic island includes an O-point in its center and a pair of X-points at its sides. These magnetic islands in the double current sheets interact with each other. Joule heating and shocks inside these islands are the possible mechanisms to heat the plasmas (Ni et al. 2015, 2016), and could further produce the bright core and extended enhanced wings (Innes et al. 2015). The velocities at two sides of magnetic islands can be reached with a fast speed of around 200 km s^{-1}, no matter if there are blue or red shifts, while the velocities in the centers of magnetic islands are slow, as shown in panel (a). However, the plasma temperature is very high in the double current sheets, especially in the magnetic islands. The plasma temperature in the center and two sides of the magnetic islands can be as high as 10^6 K (panel b), which is much higher than the formation temperature of Si IV 1402.77 Å, i.e., 8×10^4 K. Therefore, we expect the radiative cooling process to decrease the temperature inside the reconnection region, as described by Λ in Equation (2).

The cooling function is defined by the number density (n) and cooling rates (see Eq. (2)), while the cooling rates ($\tilde{\Lambda}$) are from the table given by Mignone et al. (2007). Figure 1 demonstrates that the cooling rates depend on temperature, which clearly indicates that the cooling rates are strongly sensitive to a temperature between about 10^4 K and 10^6 K. This is just what we are interested in, as the formation temperature of Si IV 1402.77 Å is exactly between them. In fact, the cooling rates are also sensitive at much higher temperature, i.e., $> 10^8$ K, but it is out of the scope of this study.

The lower panels in Figure 2 depict the MHD simulation results with the radiative cooling process at $t = 22$ s. Similar to the upper panels in Figure 2, multiple magnetic islands with O-points in their centers and X-points at their two sides appear, which interact with each other. The velocities at the two sides of the magnetic islands can be around 200 km s^{-1}, while the velocities in the centers of the magnetic islands are slow, as shown in panel (d). Moreover, the plasma temperature in the reconnection region is decreasing, but the number density is increasing at the same time. The plasma temperature in the double current sheets is cooling down to form the Si IV 1402.77 Å line, i.e., in the centers and two sides of the magnetic islands.

3.2 Synthesized Line Profiles

Using Equation (4) and the simulation variables, we can synthesize the line profiles of Si IV 1402.77 Å, as depicted in Figure 3. Here, the velocity distribution (Vel) is the velocity (v) on the left side of Equation (4), and the final value of intensity for each given v (Vel) as shown in Figure 3 is then calculated by integrating the intensity $I(v)$ along the x axis. Panel (e) demonstrates the evolution of the spectral line with time in the case with radiative cooling. At the beginning of $t \approx$ 0–5 s, only the line core is bright, and it is also very narrow. Then the line core becomes broader and broader with time, such as at $t \approx$ 5–15 s. Next, two extended line wings appear to brighten and move to blue and red wings simultaneously, i.e., $t \approx$ 15–85 s, and the maximum speed can reach up to nearly

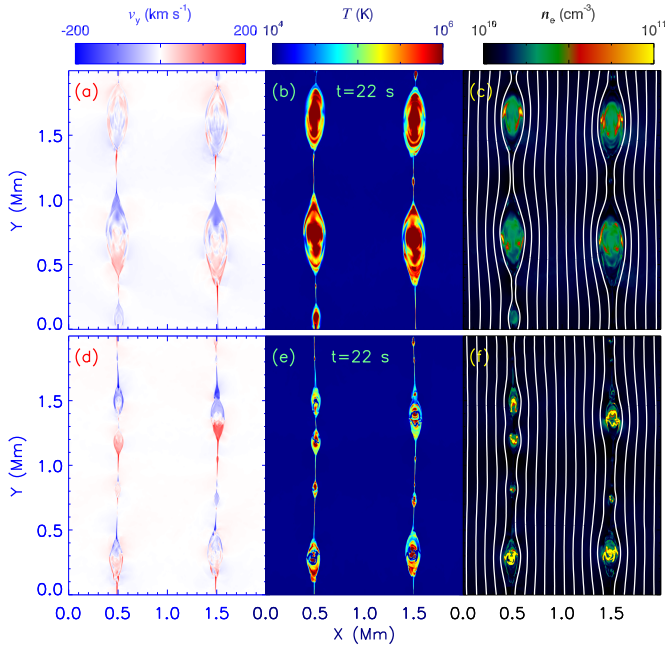

Fig. 2 The MHD simulation results without (*upper*) and with (*lower*) cooling process at $t = 22$ s: velocity (a, d), plasma temperature (b, e) and number density (c, f). The white profiles represent the magnetic field lines.

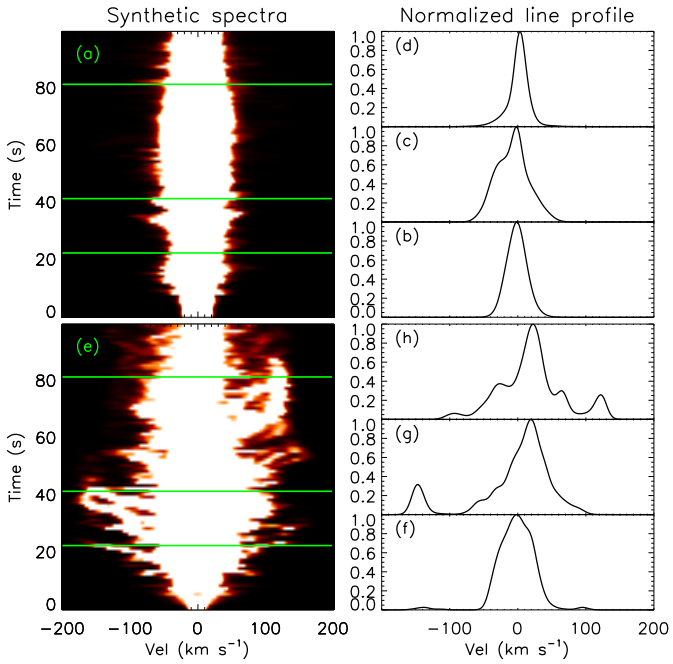

Fig. 3 Line profiles obtained from the 2-D MHD simulations. *Left*: time evolution for the line profiles of Si IV 1402.77 Å without (a) and with (e) the cooling process. *Right*: Line profiles indicated by the *green horizontal lines* in the left panel.

200 km s^{-1}, as can be seen in panels (g) and (h). Finally, both blue and red wings of the line profiles disappear, leaving only the bright and narrow core, i.e., $t \approx 85$–100 s. During the time interval between $t \approx 15$–85 s, the spectral line is always non-Gaussian and asymmetrical, and the line core is brighter than its two extended wings, while the blue and red wings become brighter and brighter from the beginning of the explosive events, but disappear at the end, see panels (g)−(h). This evolution of line profiles is very similar to that of the transition-region explosive events ob-

served by *IRIS* (see Innes et al. 2015). On the other hand, the duration of this time interval is about 70 s, which is also similar to the lifetime of the transition-region explosive events in spectroscopic observations (e.g., Dere et al. 1989; Dere 1994; Ning et al. 2004; Innes et al. 2015).

To compare the simulation results with and without the cooling process, we also calculate the spectral line in the case without radiative cooling by using Equation (4), as shown in the upper panels in Figure 3. Panel (a) demonstrates the evolution of the spectral line with time, and panels (b)–(d) display the line profiles at three times. All these panels show that the spectral line is symmetrical and has a Gaussian profile in most of the simulation times. The line core is always bright and broad, but the two extended wings do not appear during our simulation times. We also notice that the line profile in panel (c) exhibits line asymmetry, but it could not be identified as the transition-region explosive event because it only brightens in the line core.

In our 2-D simulation, the small-scale magnetic reconnection produces the O-point centers with a slow speed and oppositely directed jets at two X-point sides with a fast speed, as indicated by the bright core and blue/red shifts in the line profiles. At the same time, the double current sheets become unstable and break up into several small plasmoids. The centers of these small plasmoids move with different velocities, and they are appear as broad and bright cores in the line profiles. Also, two sides of these small plasmoids move toward opposite directions with a fast speed, and they are the blue/red shifts in the line profiles, as seen in Figure 3. The blue and red shifts of the line profiles can reach nearly 200 km s^{-1}, but the bright core of the line profiles only exhibits a slow velocity, and becomes broader and broader with time. Our simulation results are very consistent with spectroscopic observations from *IRIS* (e.g., Innes et al. 2015).

3.3 The Cooling Process

The key point of our 2-D MHD simulation is the cooling process, since we aim to simulate the transition-region explosive event in Si IV 1402.77 Å that is characterized by a fast velocity but a low temperature. As shown in the upper panels of Figure 2, although the velocity at the two sides of the magnetic islands is nearly 200 km s^{-1}, the plasma temperature at these regions is very high, and the highest temperature could be nearly 10^6 K. Moreover, the plasma temperature in the centers of the magnetic islands is also as high as $\sim 10^6$ K. Such a high temperature is far more than the formation temperature of Si IV 1402.77 Å, i.e., $\sim 8\times 10^4$ K. Therefore, in order to synthesize the Si IV 1402.77 Å line profiles, we introduce the cooling function (Λ) in the energy conservation equation (see Equation (1)). Thus, it is possible to synthesize the line profile of Si IV 1402.77 Å under the condition of fast velocity and low temperature. Figure 2 depicts the MHD simulation results at $t = 22$ s without (upper) and with (lower) cooling functions, which indicate that the cooling function is working at the early stage of the explosive event.

Figures 4 and 5 further display our MHD simulation results without and with the cooling process at the middle and end times of the explosive event, such as $t = 41$ s and $t = 81$ s, respectively. Their line profiles are shown in Figure 3(c)−(d) and (g)−(h), respectively. The simulation results demonstrate that the double current sheets become broader and broader with time if there is no cooling process, and the plasma temperature in the reconnection regions is too hot to produce the line profile of Si IV 1402.77 Å, including the center and two sides of the magnetic islands. However, when we introduce the cooling function, the plasma temperature is cooling down, both at the centers and two sides of the magnetic islands. Therefore, we can synthesize the Si IV 1402.77 Å line profiles from the 2-D MHD simulation results. Figure 3 (lower) depicts the synthetic line profiles in Si IV 1402.77 Å. It exhibits a broad non-Gaussian profile (f, g and h) with a bright core and two extended (blue/red) wings (g and h).

4 CONCLUSIONS AND DISCUSSIONS

Using the PLUTO code, we perform a 2-D MHD simulation of the small-scale magnetic reconnection in double current sheets. Then using the simulation variables, such as LOS velocity, number density and plasma temperature, we synthesize the line profiles of Si IV 1402.77 Å. The spectral line shows a broad non-Gaussian profile. It is complex with a bright core and two asymmetrical extended wings (blue or red shifts with velocity of nearly 200 km s^{-1}), and this process can last for $\sim$70 s, as displayed in Figure 3. All these line features agree well with transition-region explosive events observed by *IRIS* (see Innes et al. 2015). Their observations show that the spectral line profiles of Si IV 1402.77 Å at small-scale acceleration sites are broad and asymmetrical. They have bright central cores and extended blue/red wings with low intensity and fast velocity over 200 km s^{-1}. The line emissions from the bright core and two extended wings are spatially coincident and neither move significantly during the lifetime of the explosive events. These observational line features can also be found in our simulation, as seen in the lower panels of

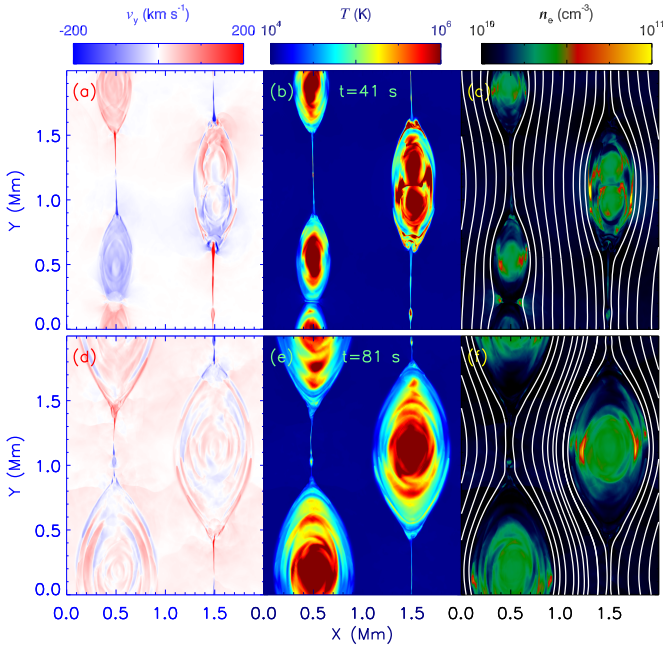

Fig. 4 Similar to the upper panels of Fig. 2, but at $t = 41$ s (*upper*) and $t = 81$ s (*lower*).

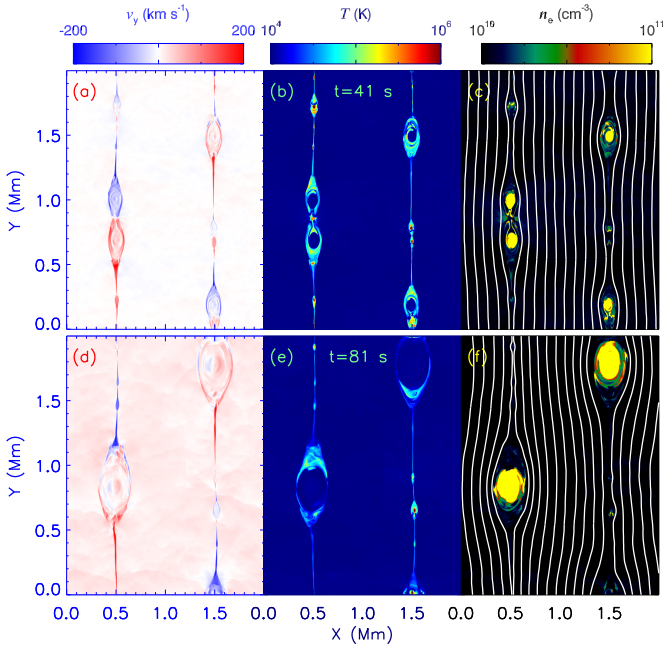

Fig. 5 Similar to the lower panels of Fig. 2, but at $t = 41$ s (*upper*) and $t = 81$ s (*lower*).

Figure 3. Here, the double current sheet configuration is used to allow periodic boundaries. As is known, the boundaries around transition-region explosive events in the solar atmosphere are definitely not periodic. Thus, the periodic boundary conditions make the plasmas flow out from one boundary and flow in from the other boundary in the y direction in this work, which affects the reconnection region and distributions of plasma temperature and density. Therefore, the synthesized spectral lines will possibly be different if other more realistic boundary conditions are applied. We will check the simulations by using an open boundary in a future work.

The explosive events with bi-directional jets observed in the transition regions are thought to be produced by

small-scale magnetic reconnection on the Sun (Innes et al. 1997). They have been studied by many authors based on spectroscopic observations (e.g., Dere 1994; Innes et al. 1997; Ning et al. 2004; Innes & Teriaca 2013; Huang et al. 2014) and MHD simulations (Jin et al. 1996; Innes & Tóth 1999; Sarro et al. 1999; Roussev et al. 2001). However, there is always a contradiction between the observations and simulations of these line profiles. For example, spectroscopic observations find that the line profiles are complex with both bright cores and faint asymmetrical wings (Dere 1994; Innes et al. 1997; Ning et al. 2004; Innes et al. 2015), while the MHD simulation results based on the Petschek model (Petschek 1964) can only reproduce the extended wing brightening (Innes & Tóth 1999; Biskamp 2000; Roussev et al. 2001). This is because the Petschek mechanism only accounts for the line wings with fast velocity, but it fails to reproduce the bright core with slow velocity since there are not enough low-speed plasmas at the diffusion region (e.g., Innes & Tóth 1999). Recent large-scale MHD simulations show that plasmas with fast speeds may reproduce the jets, but plasmas with slow speeds are outside of the diffusion region (Heggland et al. 2009; Ding et al. 2011). Inspired by that, Innes et al. (2015) demonstrate that the bright core of a line profile is from heating the background plasmas. That is to say, the emissions from jets and backgrounds are spatially offset, and this can result in spatial offsets between the line core and brightening of the two extended wings. This reconnection model can explain the bright core and extended wings very well. Our 2-D MHD simulations of magnetic reconnection show a rapid growth of the magnetic islands along the double current sheets. These magnetic islands are divided by the fast jets and can explain well the bright core and extended wings of the line profiles in the explosive events. Therefore, we conclude that the transition-region explosive events with a bright core and two extended wings are most likely produced by the plasmoid instability rather than the Petschek mechanism (Petschek 1964) during small-scale magnetic reconnection on the Sun. The bright emission of a line core is contributed from the high-density and low-velocity magnetic islands, as shown in Figures 2 (lower) and 5.

As mentioned in Section 3.3, the key point of our 2-D MHD simulation is the cooling process. In this paper, optically thin radiative cooling is considered, which is dependent on the cooling rates and number density (see Eq. (2)). The tabulated cooling rates (see Fig. 1) are used to decrease the plasma temperature inside the reconnection region, and they seem to work well (e.g., Figs. 4 and 5), especially at the temperature region between 10^4 K and 10^6 K (see also Schmutzler & Tscharnuter 1993; Teşileanu et al. 2008). Thermal conduction is neglected in our 2-D MHD simulation. We do not know if heat conduction will play a role in our 2-D simulation, and this will be checked in a future work. On the other hand, we apply an initial uniform density of $10^{10}\,\mathrm{cm}^{-3}$ in the simulation, which can result in a maximum density of $\sim 10^{11}\,\mathrm{cm}^{-3}$. This value is consistent with the number density in the transition region on the Sun. Therefore, our 2-D MHD simulation conditions are very close to the situations in the solar transition region, and our simulation results agree well with the *IRIS* spectroscopic observations (see Innes et al. 2015). In fact, Innes et al. (2015) already synthesized the line profile of Si IV 1402.77 Å by using 2-D simulation results of magnetic reconnection with plasmoid instabilities, but radiative cooling is not included in their simulations. We add the radiative cooling process in our 2-D MHD simulations and obtain similar results. In the future, we wish to work together with them using their method and code.

Innes et al. (2015) firstly successfully applied the reconnection process with plasmoid instability to explain the Si IV line profile in the transition region events. The characteristic parameters and initial conditions in their 2-D simulation have been described, i.e., the plasma density, magnetic field and temperature in the inflow regions are set to be $10^{10}\,\mathrm{cm}^{-3}$, 12 G and 2×10^5 K respectively. In our 2-D simulations, the initial plasma density, magnetic field and temperature are $10^{10}\,\mathrm{cm}^{-3}$, 10 G and 2.4×10^4 K, respectively. Therefore, the initial plasma beta (β=0.02) in this work is about five times smaller than that (β=0.1) in the inflow region of Innes et al. (2015). In Innes et al. (2015), a Harris current sheet is applied as the initial configuration of the magnetic field (Guo et al. 2014), which makes the initial plasma density and pressure non-uniform across the current sheet. The initial plasma density and plasma beta in the center of the current sheet are higher than those in the inflow region. As shown in Equation (3) in our simulation, the absolute value of the initial magnetic field is uniform across the current sheet, which makes the initial plasma density and pressure also uniform. Therefore, the different initial plasma beta (β) and initial configurations of magnetic field, plasma density and pressure are possible reasons causing the huge difference in plasma heating between our work and that of Innes et al. (2015). The plasma in the simulation work of Innes et al. (2015) is not strongly heated as shown in our work, and the maximum plasma temperature in Innes et al. (2015) only reaches the characteristic value of 2×10^5 K. Therefore, the

Si IV line profile can be synthesized well by using their 2-D simulation results without radiative cooling. Therefore, radiative cooling is possibly not important in some of the transition region reconnection events.

In our 2-D simulation, the magnetic diffusion is set as a constant, and the highest resolution is (64×2^4)*(64×2^4). We know that the resolution must be high enough in the simulations, otherwise the numerical diffusion will be higher than the magnetic diffusion set in the MHD equations and the numerical diffusion instead of magnetic diffusion dissipates the magnetic energy. Therefore, a higher refinement level is used in our 2-D simulation, such as (64×2^5)*(64×2^5). In addition, the simulation results by using a higher refinement level are very similar to those in our above work, i.e., the plasma temperatures both in the centers and at two sides of magnetic islands are cooling down. Therefore, the resolution in our work is high enough in our work.

Acknowledgements We acknowledge the anonymous referee for his/her inspiring suggestions and constructive comments. The author would like to thank Dr. D. E. Innes for her valuable suggestions for completing this paper. PLUTO is a freely-distributed software package for the numerical solution of mixed hyperbolic/parabolic systems of partial differential equations (conservation laws) targeting high Mach number flows in astrophysical fluid dynamics. This study is supported by the National Natural Science Foundation of China (Grant Nos. 11603077, 11573072, 11790302 and 11333009 and U1731241), the CRP (KLSA201708), the Youth Fund of Jiangsu (Nos. BK20161095 and BK20171108) and the Strategic Priority Research Program on Space Science, CAS (Nos. XDA15052200 and XDA15320301). The associated Laboratory (No. is 2010DP173032).

References

Aschwanden, M. J. 2002, Space Sci. Rev., 101, 1
Bhattacharjee, A., Huang, Y.-M., Yang, H., & Rogers, B. 2009, Physics of Plasmas, 16, 112102
Biskamp, D. 2000, Magnetic Reconnection in Plasmas (Cambridge: Cambridge University Press)
Brueckner, G. E., & Bartoe, J.-D. F. 1983, ApJ, 272, 329
Cheng, X., Ding, M. D., & Fang, C. 2015, ApJ, 804, 82
Curdt, W., & Tian, H. 2011, A&A, 532, L9
De Pontieu, B., Title, A. M., Lemen, J. R., et al. 2014, Sol. Phys., 289, 2733
Del Zanna, G., Dere, K. P., Young, P. R., Landi, E., & Mason, H. E. 2015, A&A, 582, A56
Dere, K. P. 1994, Advances in Space Research, 14, 13
Dere, K. P., Bartoe, J.-D. F., & Brueckner, G. E. 1989, Sol. Phys., 123, 41
Dere, K. P., Bartoe, J.-D. F., Brueckner, G. E., Ewing, J., & Lund, P. 1991, J. Geophys. Res., 96, 9399
Ding, J. Y., Madjarska, M. S., Doyle, J. G., et al. 2011, A&A, 535, A95
Guo, L.-J., Bhattacharjee, A., & Huang, Y.-M. 2013, ApJ, 771, L14
Guo, L.-J., Huang, Y.-M., Bhattacharjee, A., & Innes, D. E. 2014, ApJ, 796, L29
Hansteen, V. H., Hara, H., De Pontieu, B., & Carlsson, M. 2010, ApJ, 718, 1070
Heggland, L., De Pontieu, B., & Hansteen, V. H. 2009, ApJ, 702, 1
Hong, J., Ding, M. D., Li, Y., et al. 2016, ApJ, 820, L17
Huang, Y.-M., & Bhattacharjee, A. 2010, Physics of Plasmas, 17, 062104
Huang, Z., Madjarska, M. S., Xia, L., et al. 2014, ApJ, 797, 88
Huang, Z., Madjarska, M. S., Scullion, E. M., et al. 2017, MNRAS, 464, 1753
Innes, D. E., Inhester, B., Axford, W. I., & Wilhelm, K. 1997, Nature, 386, 811
Innes, D. E., & Tóth, G. 1999, Sol. Phys., 185, 127
Innes, D. E. 2001, A&A, 378, 1067
Innes, D. E., & Teriaca, L. 2013, Sol. Phys., 282, 453
Innes, D. E., Guo, L.-J., Huang, Y.-M., & Bhattacharjee, A. 2015, ApJ, 813, 86
Jiang, J., Hathaway, D. H., Cameron, R. H., et al. 2014, Space Sci. Rev., 186, 491
Jin, S.-P., Inhester, B., & Innes, D. 1996, Sol. Phys., 168, 279
Khomenko, E., & Collados, M. 2012, ApJ, 747, 87
Klassen, A., Gómez-Herrero, R., & Heber, B. 2011, Sol. Phys., 273, 413
Li, C., Tang, Y. H., Dai, Y., Fang, C., & Vial, J.-C. 2007, A&A, 472, 283
Li, C., Dai, Y., Vial, J.-C., et al. 2009, A&A, 503, 1013
Li, D., & Ning, Z. 2012, Ap&SS, 341, 215
Li, D., Ning, Z., & Su, Y. 2016a, Ap&SS, 361, 301
Li, L., Zhang, J., Peter, H., et al. 2016b, Nature Physics, 12, 847
Li, Y., & Ding, M. D. 2017, ApJ, 838, 15
Li, D. 2017, RAA (Research in Astronomy and Astrophysics), 17, 040
Li, D., Li, L., & Ning, Z. 2018, MNRAS, 479, 2382
Lin, J., Ko, Y.-K., Sui, L., et al. 2005, ApJ, 622, 1251
Liu, R., Lee, J., Wang, T., et al. 2010, ApJ, 723, L28
Liu, W., Chen, Q., & Petrosian, V. 2013, ApJ, 767, 168
Masuda, S., Kosugi, T., Hara, H., Tsuneta, S., & Ogawara, Y. 1994, Nature, 371, 495
Mignone, A., Bodo, G., Massaglia, S., et al. 2007, ApJS, 170, 228
Mignone, A., Zanni, C., Tzeferacos, P., et al. 2012, ApJS, 198, 7
Ni, L., Roussev, I. I., Lin, J., & Ziegler, U. 2012, ApJ, 758, 20
Ni, L., Kliem, B., Lin, J., & Wu, N. 2015, ApJ, 799, 79
Ni, L., Lin, J., Roussev, I. I., & Schmieder, B. 2016, ApJ, 832,

195
Ning, Z., Innes, D. E., & Solanki, S. K. 2004, A&A, 419, 1141
Ning, Z., & Guo, Y. 2014, ApJ, 794, 79
Pérez, M. E., Doyle, J. G., Erdélyi, R., & Sarro, L. M. 1999, A&A, 342, 279
Petschek, H. E. 1964, NASA Special Publication, 50, 425
Priest, E. R., Parnell, C. E., & Martin, S. F. 1994, ApJ, 427, 459
Roussev, I., Galsgaard, K., Erdélyi, R., & Doyle, J. G. 2001, A&A, 370, 298
Sarro, L. M., Erdélyi, R., Doyle, J. G., & Pérez, M. E. 1999, A&A, 351, 721
Schmutzler, T., & Tscharnuter, W. M. 1993, A&A, 273, 318
Shen, C., Lin, J., & Murphy, N. A. 2011, ApJ, 737, 14
Shen, Y., Liu, Y., Liu, Y. D., et al. 2015, ApJ, 814, L17
Su, Y., Veronig, A. M., Holman, G. D., et al. 2013, Nature Physics, 9, 489
Sun, X., Hoeksema, J. T., Liu, Y., Chen, Q., & Hayashi, K. 2012, ApJ, 757, 149
Sun, J. Q., Cheng, X., Ding, M. D., et al. 2015, Nature Communications, 6, 7598
Teşileanu, O., Mignone, A., & Massaglia, S. 2008, A&A, 488, 429
Tian, H. 2017, RAA (Research in Astronomy and Astrophysics), 17, 110
Tian, H., Li, G., Reeves, K. K., et al. 2014, ApJ, 797, L14
Tian, H., Zhu, X., Peter, H., et al. 2018, ApJ, 854, 174
Wilhelm, K., Marsch, E., Dwivedi, B. N., & Feldman, U. 2007, Space Sci. Rev., 133, 103
Winebarger, A. R., Emslie, A. G., Mariska, J. T., & Warren, H. P. 1999, ApJ, 526, 471
Winebarger, A. R., Emslie, A. G., Mariska, J. T., & Warren, H. P. 2002, ApJ, 565, 1298
Xue, Z., Yan, X., Cheng, X., et al. 2016, Nature Communications, 7, 11837
Xue, Z., Yan, X., Yang, L., et al. 2018, ApJ, 858, L4
Yan, X. L., Yang, L. H., Xue, Z. K., et al. 2018, ApJ, 853, L18
Yang, L.-P., Wang, L.-H., He, J.-S., et al. 2015a, RAA (Research in Astronomy and Astrophysics), 15, 348
Yang, S., & Zhang, J. 2014, ApJ, 781, 7
Yang, S., Zhang, J., & Xiang, Y. 2015b, ApJ, 798, L11
Yuan, D., Su, J., Jiao, F., & Walsh, R. W. 2016, ApJS, 224, 30
Zhang, Q. M., Chen, P. F., Guo, Y., Fang, C., & Ding, M. D. 2012, ApJ, 746, 19
Zhao, J., & Li, H. 2012, RAA (Research in Astronomy and Astrophysics), 12, 1681
Zhao, J., Schmieder, B., Li, H., et al. 2017, ApJ, 836, 52